*Article*

# Synthesis of Ergosterol Peroxide Conjugates as Mitochondria Targeting Probes for Enhanced Anticancer Activity

**Ming Bu [1],\*, Hongling Li [1], Haijun Wang [1], Jing Wang [1], Yu Lin [1] and Yukun Ma [2]**

[1]    College of Pharmacy, Qiqihar Medical University, Qiqihar 161006, China; LHL28@qmu.edu.cn (H.L.); wanghaijun@qmu.edu.cn (H.W.); qyyx305@qmu.edu.cn (J.W.); linyu7373@163.com (Y.L.)

[2]    Research Institute of Medicine & Pharmacy, Qiqihar Medical University, Qiqihar 161006, China; mayukun@qmu.edu.cn

\*    Correspondence: buming@qmu.edu.cn; Tel.: +86-0452-2663-881

check for updates

**Abstract:** Inspired by the significant bioactivity of ergosterol peroxide, we designed and synthesized four fluorescent coumarin and ergosterol peroxide conjugates **8a–d** through the combination of ergosterol peroxide with 7-*N,N*-diethylamino coumarins fluorophore. The cytotoxicity of synthesized conjugates against three human cancer cells (HepG2, SK-Hep1, and MCF-7) was evaluated. The results of fluorescent imaging showed that the synthesized conjugates **8a–d** localized and enriched mainly in mitochondria, leading to significantly enhanced cytotoxicity over ergosterol peroxide. Furthermore, the results of biological functions of **8d** showed that it could suppress cell colony formation, invasion, and migration; induce G2/M phase arrest of HepG2 cells, and increase the intracellular ROS level.

**Keywords:** ergosterol peroxide; target probe; mitochondria; fluorescence imaging; antitumor activity

## 1. Introduction

Sterols are the important active ingredients of plants or fungal secondary metabolites. Steroidal compounds have drawn attention not only due to unusual and interesting chemical structures but also due to their widespread application as anti-inflammatory, diuretic, anabolic, and anticancer agents [1–4]. Sterol 5$\alpha$,8$\alpha$-endoperoxides are a kind of important active substances in drug discovery, which all have a unique 5$\alpha$,8$\alpha$-peroxy moiety (peroxidic bond or peroxide bridge) in the parent structure [5–10]. Ergosterol peroxide (5$\alpha$,8$\alpha$-epidioxiergosta-6,22-dien-3$\beta$-ol, EP, **1**) is a member of a class of fungal secondary metabolites of sterol endoperoxide derivatives and has been constantly discovered and extracted from different sources of medicinal fungi (Figure 1A) [11–14]. It has been reported that ergosterol peroxide can inhibit tumor cells growth by anti-angiogenesis or cytotoxicity [15–19].

In our previous study, we obtained pure ergosterol peroxide by chemical extraction and separation from *Ganoderma lucidum*. As the isolated amount of ergosterol peroxide from natural sources is not sufficient for an in-depth study on it, we got an effective chemical method to synthesize ergosterol peroxide (Figure 1). The synthesis of ergosterol peroxide was achieved by the treatment of natural ergosterol with oxygen in the presence of visible light and photosensitive catalysis [20–22]. Also, we have proved that ergosterol peroxide could inhibit forkhead-box O3 transcription factor (Foxo3a) functions by the inhibition of phosphorylate protein kinase (pAKT) to induce tumor cell death [23].
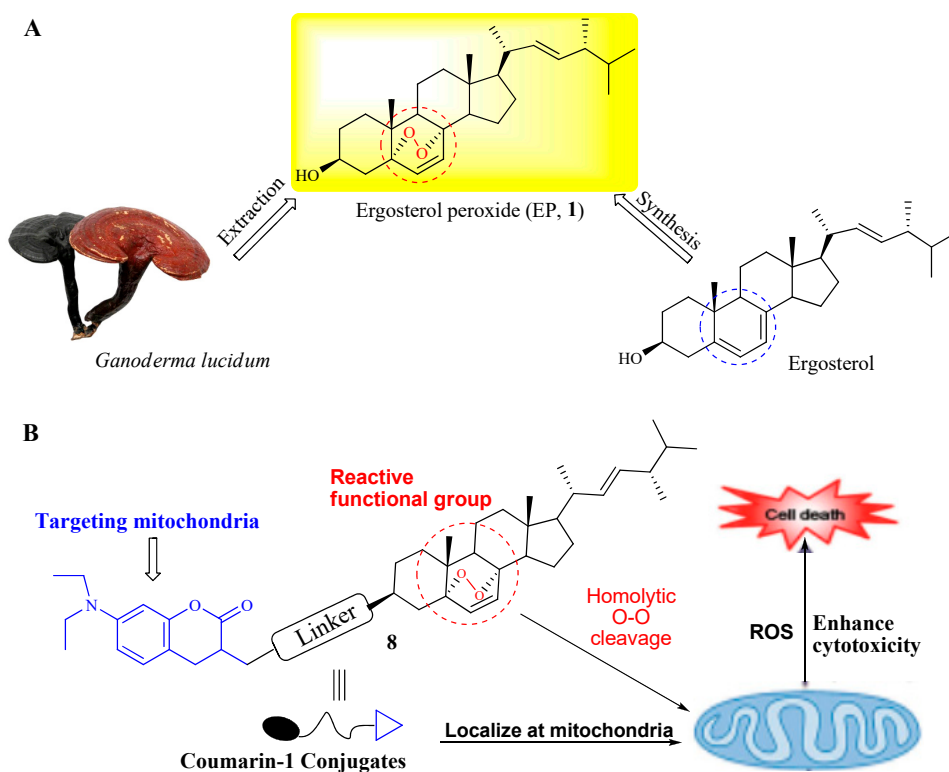
**Figure 1.** The chemical structures of compounds and design strategy. (**A**) The chemical structure and source of ergosterol peroxide (**1**). (**B**) The chemical structure of designed coumarin-**1** conjugates **8**, and the proposed mechanism of **8** for intracellular tracking and cancer-cell therapy.

Natural ergosterol, which is lacking a peroxidic bond (O-O), has been proved with no significant activity against most of the cancer cells [24]. Hence, it is generally accepted that the peroxide bridge is a crucial functional group to the biological activities [25,26]. The hemolytic cleavage of the peroxide bridge in a reducing environment induces reactive oxygen species (ROS), which could be cytotoxic to cancer cells [27–30].

Selective delivery of drug probes to subcellular organelles in tumor cells has emerged as an effective and attractive strategy for cancer therapy. It exerts synchronous tumor targeting and molecular imaging of drug delivery. Therefore, various theranostic probes that target different subcellular organelles in cancer cells, including the endoplasmic reticulum, lysosomes, and mitochondria, have been continuously reported in recent years [31–33]. Among them, mitochondria represent the most attractive target for effective theranostic probe development due to their key role in controlling many essential functions in cancer cells. The specific motivation of inducing mitochondrial dysfunctions has been acknowledged as an effective method in cancer therapy [34–37].

Herein, we designed four fluorescent coumarin and ergosterol peroxide conjugates **8a–d** through the combination of ergosterol peroxide with different targeting coumarin-3-carboxamide analogs. We postulated that the mitochondria-targeting coumarin analogs could efficiently take ergosterol peroxide selective accumulated in mitochondria, in which subsequent production of ROS from the hemolytic cleavage of the endoperoxide bond in ergosterol peroxide would induce mitochondrial dysfunction and kill tumor cells (Figure 1B).

## 2. Results and Discussion

### 2.1. Chemistry

First, using ergosterol (EG) as material, we achieved a chemical synthesis of ergosterol peroxide by the treatment of ergosterol in the presence of eosin Y, oxygen, and visible light (Scheme 1) [22].
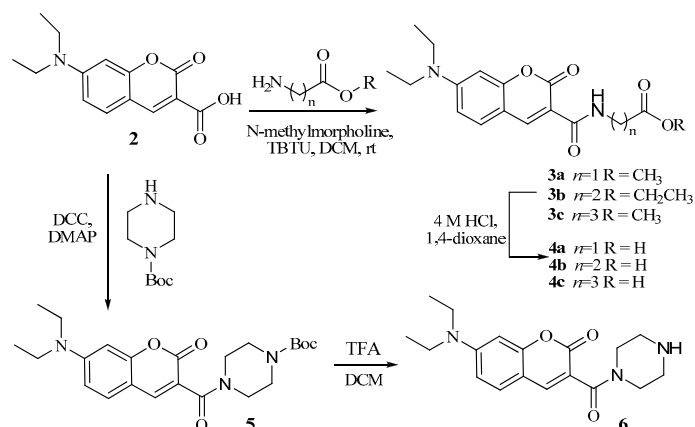
**Scheme 1.** Synthesis of coumarin analogs **4a–c** and **6**.

There is a hydroxyl group at the C-3 position of ergosterol peroxide that is also a feasible functional site. We designed and synthesized four ergosterol peroxide-coumarin conjugates **8a–d** to evaluate the biological activities of various groups of linker at the C-3 position. The reason for the use of amino acids as spacers is that the amide bond is fairly stable, and the synthesis of compounds in which the amide bond is formed by coupling reagents is simple. Thus, three different amino acids (glycine, β-alanine, or γ-aminobutyric acid) were selected as the linker, to increase the space distance between ergosterol peroxide and coumarin fluorophore.

The synthetic routes of different coumarin fluorophore analogs are presented in Scheme 2. 2.7-(*N,N*-Diethylamino)coumarin-3-carboxylic acid (**2**) was generated according to known procedures [38]. Three different amino acid esters were introduced to the carboxyl group of compound **2** for amide bond formation by the same acylation reaction to give compounds **3a–c**. Then, the ester protecting a group of compounds **3a–c** could be hydrolyzed with an aqueous solution of hydrochloric acid to give three coumarin fluorophore carboxylic acid analogs **4a–c**. Besides, as a comparison, we also synthesized an ergosterol peroxide and fluorophore conjugate **6** with piperazine as the linker.
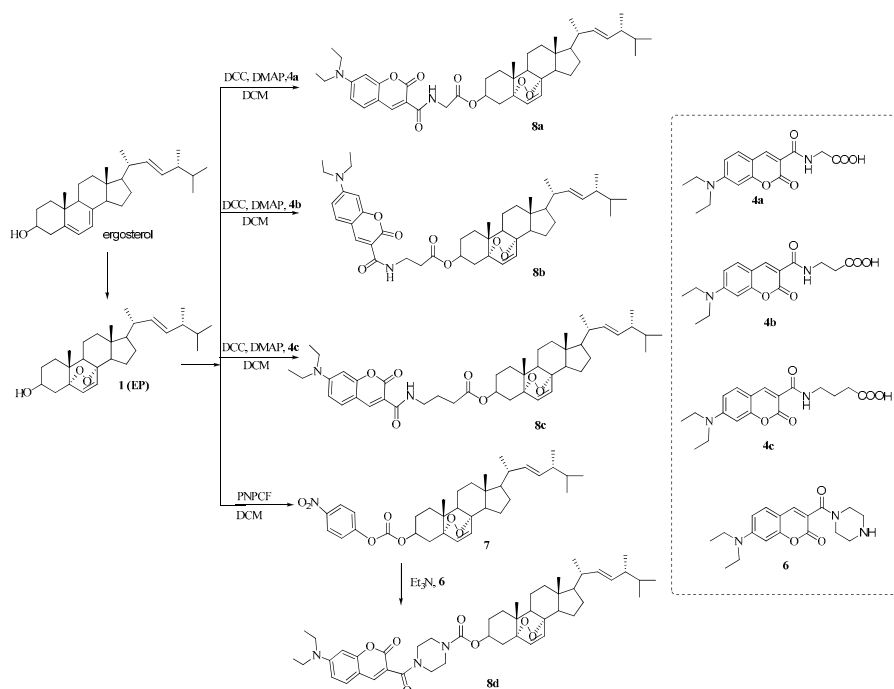


**Scheme 2.** Synthesis of coumarin and ergosterol peroxide conjugates **8a–d**.

Finally, conjugates **8a–c** were obtained by introducing ergosterol peroxide directly to the carboxylic group of **4a–c**, using dicyclohexylcarbodi imide (DCC) as the coupling reagent (Scheme 2). Also, ergosterol peroxide was reacted with 4-nitrophenyl chloroformate using pyridine as the base in dichloromethane to get intermediate **7**. Then, **7** reacted with intermediate **6** to obtain the desired conjugate **8d**.

## 2.2. Optical Properties and Subcellular Localization

First, the optical properties of four ergosterol peroxide conjugates **8a–d** were investigated (Table 1). In general, all four conjugates possess typical optical properties [39]. Especially, probe **8d** with a maximum excitation wavelength ($\lambda_{ex}$) of about 469.5 nm and an emission wavelength ($\lambda_{em}$) of about 404 nm. The large Stokes shift (65.5 nm) of probe **8d** ensured ideal photophysical properties for living cells fluorescence imaging studies. Thus, probe **8d** was chosen for further subcellular localization study.

**Table 1.** Photophysical data for probes **8a–d** and **2** [a].

| Entry | Probe | $\lambda_{ex}$ (nm) [b] | $\lambda_{em}$ (nm) [c] | Stokes Shift (nm) |
|---|---|---|---|---|
| 1 | **8a** | 479 | 422.5 | 56.5 |
| 2 | **8b** | 475 | 422 | 53 |
| 3 | **8c** | 476 | 421.5 | 54.5 |
| 4 | **8d** | 469.5 | 404 | 65.5 |
| 5 | **2** | 470.5 | 406 | 64.5 |

[a] Determined in DMSO (1 μM in DMSO). [b] Excitation maxima. [c] Emission maxima.

The subcellular localization of probe **8d** in living HepG2 cells was carried with the green mitochondria-specific dye Rhodamine 123 (Rh123) as a comparison ($\lambda_{ex}$ = 488 nm, $\lambda_{em}$ = 515–530 nm) [40]. The intracellular microscopic fluoroscope imaging was captured by Carl Zeiss 710M confocal laser scanning microscopy. As shown in Figure 2A,B, HepG2 cells were universality stained by **8d** (5 μM and 10 μM) after 2 h of incubation. Bright blue fluorescence was captured successfully in HepG2 cells ($\lambda_{ex}$ = 430–500 nm), which demonstrated both satisfactory permeability into the cell membrane and high cellular uptake of **8d**. What's more, the extensive merged blue-green color fluorescence images illustrated that probe **8d** could strongly co-localize with specific dye Rh123 in mitochondria. Also, as shown in Figure 2C,D, MCF-7 cells were successfully stained by **8c** or **8d** (10 μM). The results suggested that the fluorescent coumarin-3-carboxamide could successfully deliver ergosterol peroxide to mitochondria.
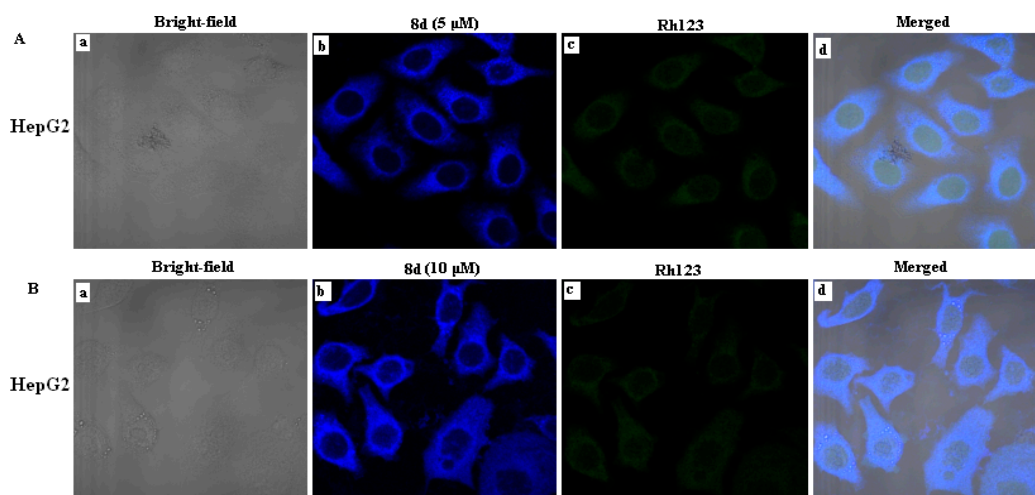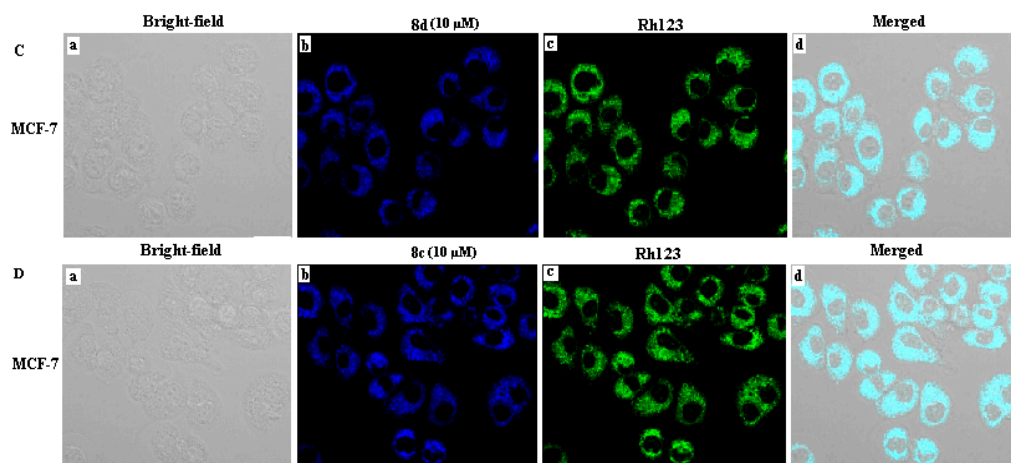


**Figure 2.** *Cont.*

**Figure 2.** Confocal laser scanning microscopic images of cancer cells treated with **8c** or **8d** in the presence of Rh123 (0.5 μM, 20 min) in PBS buffer. (**A**) Fluorescence images of HepG2 cells stained with **8d** (5 μM). (**B**) Fluorescence images of HepG2 cells stained with **8d** (10 μM). (**C**) Fluorescence images of MCF-7 cells stained with **8d** (10 μM). (**D**) Fluorescence images of MCF-7 cells stained with **8c** (10 μM). (**a**) Cell images in bright-field. (**b**) Fluorescence images of cells stained with **8c** or **8d**. (**c**) Fluorescence images of cells stained with Rh123. (**d**) Merged images of (**b**) and (**c**). All images were acquired under a 20× objective lens.

## 2.3. Biological Evaluation

### 2.3.1. Cytotoxic Activity

The newly synthesized conjugates **8a–d** and ergosterol peroxide were evaluated for their cytotoxicities against human hepatic carcinoma cells (HepG2, Sk-Hep2) and human breast cancer cells (MCF-7) by the MTT (3-(4,5-dimethylthiazol-2-yl)-2,5-diphenyltetrazolium bromide) assay. Cisplatin was chosen as a positive control drug. The results in Table 2 show that all conjugates have ideal cytotoxicity to these three tumor cell lines, with half maximal inhibitory concentration ($IC_{50}$) values at the sub-micromolar levels. Among them, probes **8c** and **8d** were the most potent to the tested cancer cells. Probe **8c** with a longer linker (γ-aminobutyric acid) had around twofold improved potency against three tested cancer cells relative to that of **8a**. Besides, probe **8d** with a special pyridine moiety as linker exhibited significant cytotoxicity against human liver cancer cells (HepG2, SK-Hep1), with $IC_{50}$ values of 6.60 μM for HepG2, which is nearly equivalent to **8c** for Sk-Hep1. Moreover, much weaker cytotoxicities were measured for either **1** or **2**, which suggested that the cytotoxicities of probes **8a–d** were associated with the synergistic effect of these two components. Overall, three probes **8b**, **8c,** and **8d** exhibited significant cytotoxicities against HepG2 cell lines, with $IC_{50}$ values lower than 10 μM. To understand the mechanism of cancer cells death caused by treatment with coumarin-**1** conjugates, we chose probe **8d** for the series of biological functions experiments.

**Table 2.** Cytotoxicities of compounds against three cancer cell lines.

| Comp. | $IC_{50}$ (μM) [a] | | |
|---|---|---|---|
| | HepG2 | SK-Hep1 | MCF-7 |
| **8a** | 12.34 ± 0.49 | 10.43 ± 0.88 | 14.80 ± 0.28 |
| **8b** | 9.46 ± 0.35 | 11.70 ± 0.28 | 13.70 ± 0.28 |
| **8c** | 6.74 ± 0.32 | 5.92 ± 0.53 | 7.45 ± 0.50 |
| **8d** | 6.60 ± 0.16 | 8.10 ± 0.28 | 10.62 ± 0.10 |
| **EP(1)** | 23.15 ± 0.18 | 19.25 ± 0.60 | 26.06 ± 0.46 |
| **2** | >100 | >100 | >100 |
| Cisplatin | 0.65 ± 0.05 | 2.42 ± 0.06 | 6.64 ± 0.16 |

[a] Data represent the mean ± SD values of three independent determinations.

### 2.3.2. Effect of Probe 8d on the Cell Cycle Distribution

The effect of probe **8d** on tumor cell cycle distribution was carried by flow cytometry. We treated HepG2 cells with probe **8d** (3 μM) for 24 h. The low concentration of **8d** was used to avoid induction of HepG2 cell death. As shown in Figure 3A, in HepG2 cells, the cell phase distribution was $49.30 \pm 1.03\%$ vs. $53.12 \pm 1.12\%$ in G0/G1 phase, $25.09 \pm 1.18\%$ vs. $33.49 \pm 1.05\%$ in S phase, and $22.89 \pm 1.17\%$ vs. $12.31 \pm 2.05\%$ in G2/M phase before and after the effect of **8d**. The G0/G1 and S phases were increased significantly before and after the effect of **8d**, suggesting a chemical effect of **8d** on cell cycle progression. Also, the number of cells decreased in G2/M phases (Figure 3).
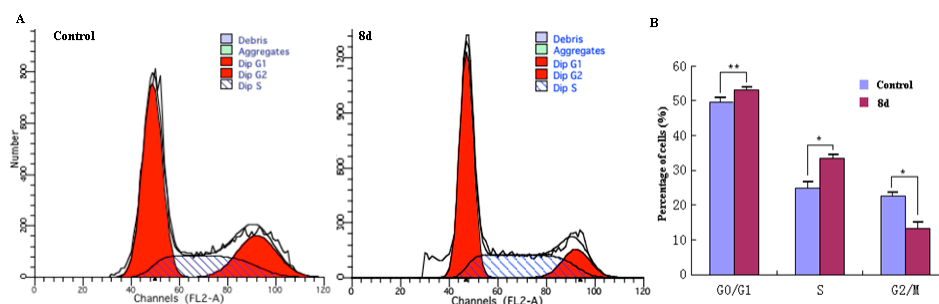


**Figure 3.** The effect of probe **8d** on the HepG2 cell cycle. (**A**) Typical distribution of cell cycles treated with or without **8d** (3 μM). (**B**) Statistical analysis of cells distributed in each phase of cell cycles. * $p < 0.05$, ** $p < 0.01$.

### 2.3.3. Effect of Probe 8d on the Cell Colony, Migration, and Invasion

The clonogenic assay is an effective method to evaluate the neoplastic transformation indirectly. Hence, we tested the effect of probe **8d** on HepG2 cells colony formation. The cells were treated with 7 μM probe **8d** for 20 days. The colony formation was observed under light microscopy. The colony numbers were $61.3 \pm 3.1$ vs. $9.1 \pm 1.4$ in HepG2 cells before and after the effect of **8d** (Figure 4). The results suggested that probe **8d** had a significant inhibitory activity to HepG2 cells growth.
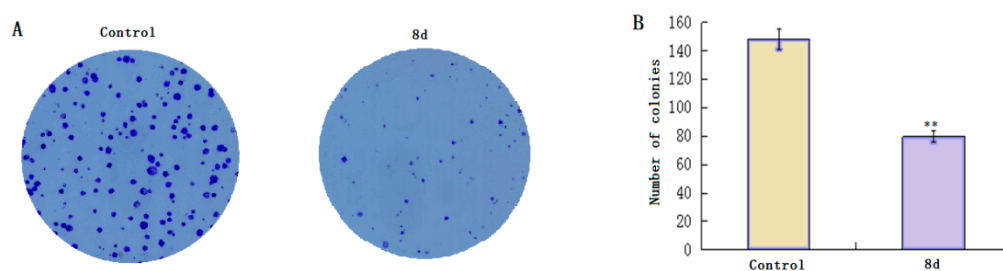


**Figure 4.** Compound **8d** inhibited cell colony formation. (**A**) Representative images of HepG2 cells colonies after treatment with **8d** (7 μM). The plates were stained with Coomassie Blue. (**B**) Data are presented as the mean ± SD of three experiments. ** $p < 0.01$.

To determine if **8d** can prevent cancer cell invasion and migration, transwell assays were performed. Under the transwell assay, the number of migratory cells was $120.4 \pm 4.2$ vs. $63.2 \pm 3.5$ for HepG2 cells before and after the effect of **8d** (6 μM). The HepG2 cell number was reduced significantly after the effect of **8d**. The results suggested that **8d** suppressed HepG2 cancer cells migration (Figure 5A,B). The number of invasive cells was $107.1 \pm 5.2$ vs. $52.7 \pm 4.6$ for HepG2 cells before and after the effect of **8d** (6 μM). The HepG2 cell number was reduced significantly after the effect of 8d. The results suggested that **8d** suppressed HepG2 cancer cell migration and invasion (Figure 5C,D).
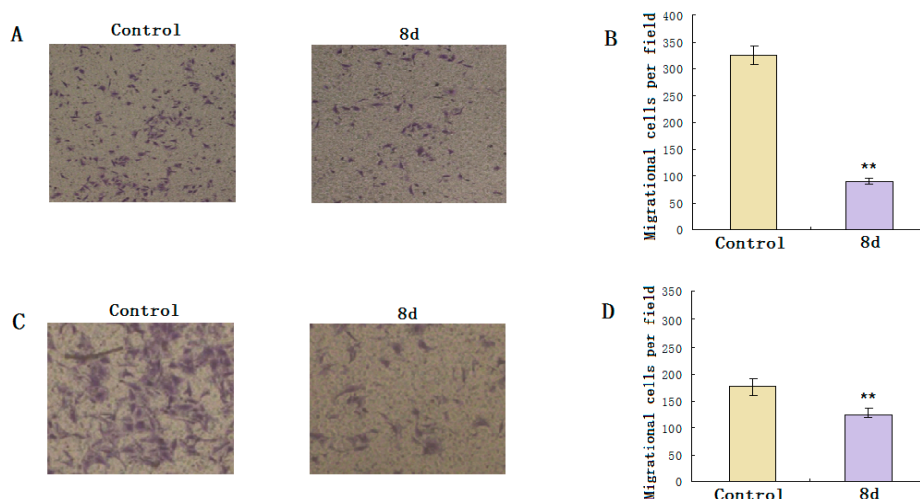
**Figure 5.** Compound **8d** suppressed HepG2 cell invasion and migration (Transwell). (**A**) Cell migration in HepG2 cells before and after the effect of **8d** (6 μM). (**B**) The migratory cell number is presented by bar diagram. (**C**) Cell invasion in HepG2 cells before and after the effect of **8d** (6 μM). (**D**) The number of cells invading to the lower chamber is presented by bar diagram. Data are presented as the mean ± SD of three experiments ** $p < 0.01$. All images were acquired under a 10× objective lens.

### 2.3.4. Effect of **8d** on the Level of ROS

To comprehend the mechanism of tumor cells death caused by treatment with probe **8d**, the level of intracellular ROS in HepG2 cells was monitored by using 5-(and-6)-chloromethyl-2′,7′-dichlorodihydrofluorescein diacetate acetyl ester (CM-H2DCFDA) as an indicator and detected by flow cytometry [41]. Figure 6 shows the effect of probe **8d** on ROS generation in HepG2 cells. A concentration-dependent increase in the ROS level was observed for HepG2 cell lines after incubation with probe **8d** (5 and 20 μM) for 24 h. The relative ROS level in HepG2 cancer cells, resulting from incubation with 20 μM probe **8d**, was about twofold higher than that of control cells without **8d**. This suggested that the intracellularly generated ROS was responsible for cell death.
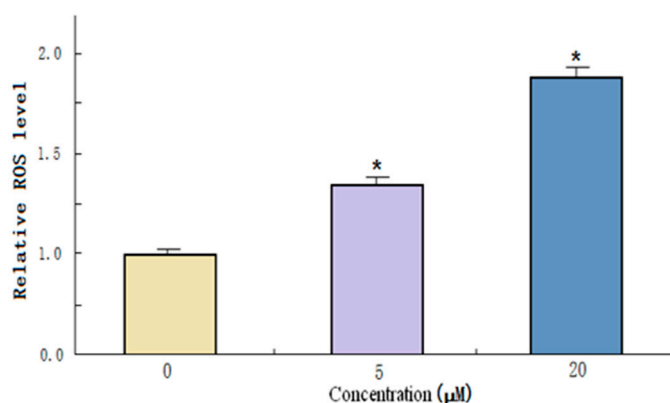


**Figure 6.** The intracellular ROS (reactive oxygen species) level of HepG2 cells was increased by treating with different concentrations of probe **8d**. Data are presented as the mean ± SD of three experiments. * $p < 0.05$.

## 3. Materials and Methods

### 3.1. Chemistry

Reagents were commercially available and used without purification. The $^1$H- and $^{13}$C-NMR spectra were recorded using the Bruker Avance DRX400 spectrometer (400 MHz and 100 MHz) in CDCl$_3$ or DMSO-$d_6$. Tetramethylsilane (TMS) was used as internal standards. Melting points were

measured by an MP120 point apparatus. Mass spectra were measured in electrospray (ESI) mode on a mass spectrometer (Esquire 6000). Flash chromatography was performed using 400 mesh silica gel. ^{1}H- and ^{13}C-NMR spectra of new compounds are available online (See Supplementary Materials).

### 3.1.1. Synthesis of Ergosterol Peroxide (1)

Ergosterol (150 mg), eosin (1 mg), and pyridine (20 mL) were added into a quartz tube. The mixture was kept in a water-cooled bath and vigorously stirred by the gas bubbling ($O_2$), radiating with an iodine tungsten lamp (500 W, 220 V) for 0.5 h. After the reaction, the mixture was poured into ice-water (20 mL) and then extracted with 50 mL ethyl acetate twice. The ethyl acetate phase was washed with 50 mL saturated brine twice and then dried with anhydrous $Na_2SO_4$. The crude product was purified by chromatographic column (ethyl acetate/petroleumether = 1/5) to get pure ergosterol peroxide as white solid [22].

### 3.1.2. Synthesis of 7-(Diethylamino)-2-Oxo-2*H*-Chromene-3-Carboxylic Acid (**2**)

2,2-Dimethyl-1,3-dioxane-4,6-dione (1.5 g, 10.36 mmol), 4-(diethylamino)-2-hydroxy-benzaldehyde (2 g, 10.36 mmol), piperidine (0.08 g, 1.04 mmol), and acetic acid (two drops) in ethanol (20 mL) was stirred for 0.5 h at room temperature, and then the mixture was heated to reflux for 4 h. After the reaction, the mixture was poured into 50 mL of ice water. The orange precipitate was collected and washed with ethanol to give **2** the crystalline solid form (63%) [38].

### 3.1.3. Synthesis of Amino-Acid Ester Derivatives

Under $N_2$, dry methanol or ethanol (100 mL) was cooled down to −5 °C, and $SOCl_2$ (21 mL, 0.3 mmol) was added dropwise. Glycine, β-alanine, or γ-aminobutyric acid (0.1 mmol) was added to this solution, and stirring was continued at room temperature for 3 h. The solvent was removed under reduced pressure to obtain the correspondent pure product as colorless crystals.

### 3.1.4. Synthesis of 2-(7-(Diethylamino)-2-Oxo-2*H*-Chromene-3-Carboxamido Ester Derivatives **3a–c**

To a stirred solution of **2** (2.42 g, 9.27 mmol) in dry dichloromethane (DCM) (160 mL), *N*-methylmorpholine (4.08 mL, 37.1 mmol) and 2-(1H-Benzotriazole-1-yl)-1,1,3,3- tetramethyluronium tetrafluoroborate (TBTU) (4.46 g, 13.9 mmol) were added. After stirring for 20 min, methyl 2-aminoacetate chloride salt (ethyl 3-aminopropanoate or methyl 4-aminobutanoate) (13.9 mmol) was added. The reaction was continued at room temperature for approximately 1.5 h under argon atmosphere. The reaction was followed on TLC chromatography plates using $CH_2Cl_2/CH_3OH$ (5/1) as the eluent. The reaction mixture was washed with a saturated water solution of $NaHSO_4$ (8 × 40 mL) and then dried with anhydrous $Na_2SO_4$. The crude product was purified by chromatographic column (10% MeOH in DCM) to give the desired products.

*Methyl 2-(7-(Diethylamino)-2-Oxo-2H-Chromene-3-Carboxamido)Acetate Ester* (**3a**): Yellow crystals (62%): mp 176–178 °C. ^{1}H-NMR (CDCl$_3$, 400 MHz) δ (ppm): 9.20 (1H, t, *J* = 5.60 Hz, -CON<u>H</u>-CH$_2$-), 8.70 (1H, s, H$^4$-Ar), 7.40 (1H, d, *J* = 8.40 Hz, H$^5$-Ar), 6.65 (1H, dd, *J* = 2.60, 8.20 Hz, H$^6$-Ar), 6.50 (1H, d, *J* = 3.60 Hz, H$^8$-Ar), 4.24 (2H, d, *J* = 6.20 Hz, -CONH-C<u>H</u>$_2$-), 3.78 (3H, s, -COO-C<u>H</u>$_3$), 3.44 (4H, q, *J* = 7.10 Hz, 2 × -C<u>H</u>$_2$CH$_3$), 1.25 (6H, t, *J* = 7.10 Hz, 2 × -CH$_2$C<u>H</u>$_3$). ^{13}C-NMR (CDCl$_3$, 100 MHz) δ (ppm): 170.54, 163.91, 162.93, 158.14, 153.09, 148.70, 131.59, 110.40, 110.04, 108.67, 96.97, 52.621, 45.48, 41.93, 12.80. MS (ESI) *m/z*: [M + H]$^+$ 333.1.

*Ethyl 3-(7-(Diethylamino)-2-Oxo-2H-Chromene-3-Carboxamido)Propanoate* (**3b**): Yellow crystals (65%): mp 129–133 °C. ^{1}H-NMR (CDCl$_3$, 400 MHz) δ (ppm): 9.09 (1H, t, *J* = 7.20 Hz, -CON<u>H</u>-CH$_2$CH$_2$-COO-), 8.71 (1H, s, H$^4$-Ar), 7.44 (1H, d, *J* = 8.90 Hz, H$^5$-Ar), 6.64 (1H, dd, *J* = 4.20, 7.70 Hz, H$^6$-Ar), 6.51 (1H, d, *J* = 3.60 Hz, H$^8$-Ar), 4.20 (2H, m, -COO-C<u>H</u>$_2$CH$_3$), 3.72–3.77 (2H, m, -CONH-C<u>H</u>$_2$CH$_2$-COO-), 3.48 (4H, q, *J* = 7.20 Hz, 2 × -C<u>H</u>$_2$CH$_3$), 2.67 (2H, m, -CH$_2$C<u>H</u>$_2$-COO-), 1.24–1.33 (9H, m, 2 × -CH$_2$C<u>H</u>$_3$, -COO-CH$_2$C<u>H</u>$_3$). ^{13}C-NMR (CDCl$_3$, 100 MHz) δ (ppm): 172.16, 163.48, 162.83, 157.95, 152.88,

148.28, 131.41, 110.46, 110.27, 108.60, 96.83, 60.97, 45.40, 35.59, 34.82, 30, 14.54, 12.78. MS (ESI) *m/z*: [M + H]$^+$ 361.2.

*Methyl 4-(7-(Diethylamino)-2-Oxo-2H-Chromene-3-Carboxamido)Butanoate* (**3c**): Yellow crystals (70%): mp 150–152 °C. $^1$H-NMR (CDCl$_3$, 400 MHz) δ (ppm): 8.82 (1H, t, *J* = 7.70 Hz, -CON<u>H</u>-CH$_2$-), 8.70 (1H, s, H$^4$-Ar), 7.43 (1H, d, *J* = 8.60 Hz, H$^5$-Ar), 6.65 (1H, dd, *J* = 4.20, 7.60 Hz, H$^6$-Ar), 6.49 (1H, d, *J* = 4.60 Hz, H$^8$-Ar), 3.67 (3H, s, -COO-C<u>H</u>$_3$), 3.42–3.52 (6H, m, 2 × -C<u>H</u>$_2$CH$_3$, -CONH-C<u>H</u>$_2$CH$_2$CH$_2$-COO-), 2.42 (2H, t, *J* = 8.20 Hz, -CONH-CH$_2$CH$_2$C<u>H</u>$_2$-COO-), 1.91–2.00 (2H, m, -CONH-CH$_2$C<u>H</u>$_2$CH$_2$-COO-), 1.24 (6H, t, *J* = 7.40 Hz, 2 × -CH$_2$C<u>H</u>$_3$). $^{13}$C-NMR (CDCl$_3$, 100 MHz) δ (ppm): 173.87, 163.61, 163.09, 157.99, 152.92, 148.41, 131.50, 110.61, 110.34, 108.73, 96.94, 51.97, 45.44, 39.22, 31.91, 25.38, 12.80. MS (ESI) *m/z*: [M + H]$^+$ 361.2.

### 3.1.5. Synthesis of 2-(7-(Diethylamino)-2-Oxo-2*H*-Chromene-3-Carboxamido)Carboxylic Acids **4a–c**

Four molar HCl (60 mL) was added dropwise into a stirred solution of **3a–c** (6 mmol) in 1,4-dioxane (120 mL). Stirring was continued at room temperature for 2 h. The reaction course was followed on TLC. The pH was adjusted to 3 with NaOH. The mixture was extracted with DCM (3 × 50 mL) and then dried with anhydrous Na$_2$SO$_4$. The crude product was purified by chromatographic column (DCM to 10% MeOH in DCM) to give the desired products **4a–c**.

*2-(7-(Diethylamino)-2-Oxo-2H-Chromene-3-Carboxamido)Acetic Acid* (**4a**): Yellow crystals (69%): mp 283–287 °C. $^1$H-NMR (CDCl$_3$, 400 MHz) δ (ppm): 12.74 (1H, s, -COO<u>H</u>), 8.98 (1H, t, *J* = 5.80 Hz, -CON<u>H</u>-CH$_2$-), 8.71 (1H, s, H$^4$-Ar), 7.73 (1H, d, *J* = 8.00 Hz, H$^5$-Ar), 6.84 (1H, m, H$^6$-Ar), 6.67 (1H, d, *J* = 2.30 Hz, H$^8$-Ar), 4.07 (2H, d, *J* = 8.20 Hz, -CONH-C<u>H</u>$_2$-), 3.51 (4H, m, 2 × -C<u>H</u>$_2$CH$_3$), 1.18 (6H, t, *J* = 7.20 Hz, 2 × -CH$_2$C<u>H</u>$_3$). $^{13}$C-NMR (CDCl$_3$, 100 MHz) δ (ppm): 172.95, 161.53, 161.41, 157.20, 152.33, 147.53, 131.48, 109.99, 109.45, 107.61, 95.84, 44.31, 43.53, 12.29. MS (ESI) *m/z*: [M + H]$^+$ 317.1.

*3-(7-(Diethylamino)-2-Oxo-2H-Chromene-3-Carboxamido)Propanoic Acid* (**4b**): Yellow crystals (71%): mp 202–205 °C. $^1$H-NMR (DMSO-*d$_6$*, 400 MHz) δ (ppm): 12.30 (1H, s, -COO<u>H</u>), 8.82 (1H, d, *J* = 8.20 Hz, -CON<u>H</u>-CH$_2$-), 8.65 (1H, s, H$^4$-Ar), 7.65–7.71 (1H, m, H$^5$-Ar), 6.65-6.83 (1H, m, H$^6$-Ar), 6.60 (1H, s, H$^8$-Ar), 3.41–3.61 (6H, m, 2 × -C<u>H</u>$_2$CH$_3$, -CONH-C<u>H</u>$_2$-), 2.45 (2H, m, -CONH-CH$_2$C<u>H</u>$_2$-COOH), 1.14 (6H, t, *J* = 7.80 Hz, 2 × -CH$_2$C<u>H</u>$_3$). $^{13}$C-NMR (DMSO-*d$_6$*, 100 MHz) δ (ppm): 174.02, 163.02, 162.51, 158.06, 153.26, 148.58, 132.40, 110.92, 110.08, 108.52, 96.69, 45.21, 35.76, 34.80, 13.16. MS (ESI) *m/z*: [M + H]$^+$ 333.1.

*4-(7-(Diethylamino)-2-Oxo-2H-Chromene-3-Carboxamido)Butanoic Acid* (**4c**): Yellow crystals (70%): mp 198–200 °C. $^1$H-NMR (DMSO-*d$_6$*, 400 MHz) δ (ppm): 12.06 (1H, s, -COO<u>H</u>), 8.62–8.66 (2H, m, -CON<u>H</u>-CH$_2$-, H$^4$-Ar), 7.67 (1H, d, *J* = 8.00 Hz, H$^5$-Ar), 6.80 (1H, dd, *J* = 3.40, 7.20 Hz, H$^6$-Ar), 6.61 (1H, d, *J* = 4.60 Hz, H$^8$-Ar), 3.48 (4H, m, 2 × -C<u>H</u>$_2$CH$_3$), 3.27–3.33 (2H, m, -CONH-C<u>H</u>$_2$CH$_2$CH$_2$-), 2.26 (2H, d, *J* = 7.80 Hz, -CONH-CH$_2$CH$_2$C<u>H</u>$_2$-COOH), 1.69–1.79 (2H, m, -CONH-CH$_2$C<u>H</u>$_2$CH$_2$-COOH), 1.14 (6H, d, *J* = 7.40 Hz, 2 × -CH$_2$C<u>H</u>$_3$). $^{13}$C-NMR (DMSO-*d$_6$*, 100 MHz) δ (ppm): 175.02, 163.11, 162.59, 158.04, 153.24, 148.45, 132.36, 110.93, 110.40, 108.53, 96.72, 45.20, 32.11, 25.65, 13.17. MS (ESI) *m/z*: [M − H]$^+$ 345.1.

### 3.1.6. Synthesis of Intermediate **6**

To a DCM solution (20 mL) of coumarin acid **2** (992.8 mg, 3.8 mmol) and mono-*t*-Boc-piperazine (1061.3 mg, 5.7 mmol), DCC (1030.0 mg, 5.0 mmol) and DMAP (6.1 mg, 0.05 mmol) were added at room temperature [41]. The solution was stirred at room temperature overnight, and then the solvent was removed under reduced pressure. The crude product was purified by chromatographic column (DCM) to give **5** as yellow solid powder (87%). Compound **6** was obtained by treatment of **5** with trifluoroacetic acid: DCM (1:1) solution. $^1$H-NMR (400 MHz, DMSO-*d$_6$*) δ (ppm): 8.89 (1H, s, NH), 8.03 (1H, s, H$^4$-Ar), 7.51 (1H, d, *J* = 8.80 Hz, H$^5$-Ar), 6.77 (1H, dd, *J* = 8.00, 3.2 Hz, H$^6$-Ar), 6.55 (1H,

d, *J* = 2.2 Hz, H$^8$-Ar), 3.67 (4H, m, 2 × -C$\underline{H}_2$CH$_3$), 3.52 (4H, m, 2 × -C$\underline{H}_2$CH$_2$NH-), 3.20 (4H, m, 2 × -CH$_2$C$\underline{H}_2$NH-), 1.13 (6H, t, *J* = 7.2 Hz, 2 × -CH$_2$C$\underline{H}_3$,). MS (ESI) *m/z*: [M + H]$^+$ 320.2.

### 3.1.7. Synthesis of Intermediate **7**

To a stirred solution of ergosterol peroxide (200 mg, 0.56 mmol) and 4-nitrophenyl chloroformate (258 mg, 1.28 mmol) in DCM (5 mL) under N$_2$ gas, pyridine (100 mg, 1.28 mmol) was added, and stirring continued at room temperature for 3 h. The reaction course was followed on TLC. Then, DCM (20 mL) and H$_2$O (20 mL) were added into the mixture. The DCM phase was combined, washed with brine, and then dried with anhydrous Na$_2$SO$_4$. The solution was concentrated to give yellow residue **7** for the next step.

### 3.1.8. Synthesis of Novel Conjugates **8a–d**

General synthesis procedure of conjugates **8a–d**: Coumarin-3-carboxylic acid derivatives **4a** (**4b**, **4c**, or **7**) (0.20 mmol), DCC (40 mg, 0.20 mmol), and DMAP (10%) were added into the solution of ergosterol peroxide (68 mg, 0.13 mmol) in DCM (20 mL). The mixture was stirred continuously at room temperature for 24~36 h. The filtrate was collected and concentrated, and the crude product was purified by chromatographic column to give target probes **8a–d**.

*2-[7-(Diethylamino)-2-Oxo-2H-Chromene-3-Carboxamido]-Glycine-3-(Ergosterol Peroxide) Probe* **8a**: Yellow powder (52%). $^1$H-NMR (400 MHz, CDCl$_3$) δ (ppm): 9.20 (1H, t, *J* = 5.4 Hz, -CON$\underline{H}$-CH$_2$-), 8.71 (1H, s, H$^4$-Ar), 7.42 (1H, dd, *J* = 8.8, 4.2 Hz, H$^5$-Ar), 6.71–6.56 (1H, m, H-6), 6.50 (2H, m, H$^6$-Ar, H$^8$-Ar), 6.25 (1H, d, *J* = 8.7 Hz, H-7), 5.25–5.14 (2H, m, H-22, H-23), 5.11 (1H, m, -O$\underline{H}$), 4.20 (2H, m, NHC$\underline{H}_2$CO), 3.46 (4H, dd, *J* = 8.2, 3.6 Hz, 2 × -C$\underline{H}_2$CH$_3$), 2.22–2.16 (1H, m), 2.11–2.06 (1H, m), 2.02 (2H, dd, *J* = 9.8, 3.3 Hz), 1.98–1.90 (2H, m), 1.85 (1H, dd, *J* = 12.9, 6.8 Hz), 1.72 (1H, m), 1.65 (4H, m), 1.58 (1H, m), 1.50 (2H, dd, *J* = 10.7, 7.2 Hz), 1.43 (1H, m), 1.34 (2H, m), 1.28-1.24 (9H, m), 1.11 (1H, m), 1.01 (3H, d, *J* = 6.6 Hz, -C$\underline{H}_3$), 0.90 (6H, m, 2 × -CH$_2$C$\underline{H}_3$), 0.82 (9H, dd, *J* = 8.3, 4.5 Hz, 3 × -C$\underline{H}_3$). $^{13}$C-NMR (100 MHz, CDCl$_3$) δ (ppm): 168.6, 163.4, 162.6, 157.8, 152.7, 148.3, 136.2, 135.1, 132.3, 131.2, 130.8, 109.9, 109.8, 108.3, 96.7, 81.8, 79.4, 70.75, 56.2, 51.6, 51.0, 45.1, 44.6, 45.1, 44.5, 42.8, 39.7, 36.9, 34.2, 33.1, 29.7, 28.6, 26.2, 23.4, 20.9, 20.6, 19.9, 19.6, 18.1, 17.6, 12.9, 12.4. MS (ESI) *m/z*: 727.4 [M + H]$^+$.

*2-[7-(Diethylamino)-2-Oxo-2H-Chromene-3-Carboxamido]-Alanine-3-(Ergosterol Peroxide) Probe* **8b**: Yellow powder (45%). $^1$H-NMR (400 MHz, CDCl$_3$) δ (ppm): 9.06 (1H, t, *J* = 5.0 Hz, -CON$\underline{H}$-CH$_2$-), 8.68 (1H, s, H$^4$-Ar), 7.42 (1H, d, *J* = 8.2 Hz, H$^5$-Ar), 6.65 (1H, m, H-6), 6.50 (2H, t, *J* = 3.6 Hz, H$^6$-Ar, H$^8$-Ar), 6.25 (1H, d, *J* = 8.4 Hz, H-7), 5.21–5.15 (2H, m, H-22, H-23), 5.05 (1H, m, -O$\underline{H}$), 3.72 (2H, m, -NHC$\underline{H}_2$CH$_2$CO-), 3.46 (4H, dd, *J* = 8.0, 3.6 Hz, 2 × -C$\underline{H}_2$CH$_3$), 2.62 (2H, t, *J* = 8.0, 3.8 Hz, -NHCH$_2$C$\underline{H}_2$CO-), 2.11 (1H, m), 2.01 (1H, m), 1.99–1.94 (4H, m), 1.71–1.60 (4H, m), 1.50 (2H, m), 1.43 (2H, m), 1.34 (2H, m), 1.28–1.24 (9H, m), 1.11 (1H, m), 1.01 (3H, d, *J* = 6.6 Hz, -C$\underline{H}_3$), 0.91 (6H, m, 2 × -CH$_2$C$\underline{H}_3$), 0.81 (9H, dd, *J* = 8.2, 4.4 Hz, 3 × -C$\underline{H}_3$). $^{13}$C-NMR (100 MHz, CDCl$_3$) δ (ppm): 170.8, 163.2, 162.5, 157.7, 152.5, 148.1, 135.2, 134.1, 132.3, 131.1, 130.8, 110.2, 109.9, 108.3, 96.6, 81.8, 79.3, 69.9, 56.2, 51.6, 51.0, 45.1, 44.6, 42.7, 39.7, 39.3, 36.9, 34.7, 33.1, 33.0, 28.6, 25.6, 25.0, 20.9, 19.9, 19.6, 18.1, 17.6, 12.9, 12.4. MS (ESI) *m/z*: 741.4 [M + H]$^+$.

*2-[7-(Diethylamino)-2-Oxo-2H-Chromene-3-Carboxamido]-Threonine-3-(Ergosterol Peroxide) Probe* **8c**: Yellow powder (52%). $^1$H-NMR (400 MHz, CDCl$_3$) δ (ppm): 8.84 (1H, s, -CON$\underline{H}$-CH$_2$-), 8.69 (1H, s, H$^4$-Ar), 7.42 (1H, d, *J* = 9.0 Hz, H$^5$-Ar), 6.65 (1H, dd, *J* = 9.0, 2.5 Hz, H-6), 6.50 (2H, dd, *J* = 5.4, 3.0 Hz, H$^6$-Ar, H$^8$-Ar), 6.23 (1H, d, *J* = 8.5 Hz, H-7), 5.18 (2H, qd, *J* = 15.3, 7.7 Hz, H-22, H-23), 5.05–4.94 (1H, m, -O$\underline{H}$), 4.12 (6H, q, *J* = 7.1 Hz, -NHC$\underline{H}_2$CH$_2$C$\underline{H}_2$CO-), 3.54–3.40 (4H, m, 2 × -C$\underline{H}_2$CH$_3$), 2.36 (2H, d, *J* = 7.7 Hz), 2.05 (3H, m), 1.95–1.92 (4H, m), 1.72–1.32 (16H, m), 1.30-1.22 (6H, m, 2 × -C$\underline{H}_3$), 1.14–1.08 (4H, m), 0.92–0.88 (6H, m, 2 × -CH$_2$C$\underline{H}_3$), 0.86–0.81 (6H, m, 2 × -C$\underline{H}_3$). $^{13}$C-NMR (100 MHz, CDCl$_3$) δ (ppm): 173.6, 164.7, 163.8, 157.6, 157.0, 153.0, 148.1, 135.2, 135.1, 132.3, 131.1, 130.8, 109.9 108.5, 96.6, 81.7, 79.4, 69.5, 56.2, 51.6, 51.0, 49.1, 45.1, 44.5, 42.8, 39.7, 39.3, 36.7, 33.9, 33.1, 32.1, 29.7, 26.4, 25.6, 24.9, 23.4, 22.8, 20.9, 19.9, 19.6, 18.1, 17.6, 12.9, 12.4. MS (ESI) *m/z*: 755.4 [M + H]$^+$.

*2-[7-(Diethylamino)-2-Oxo-2H-Chromene-3-Carboxamido]-Piperazine-3-(Ergosterol Peroxide) Probe* **8d**: Yellow powder (49%). $^{1}$H-NMR (400 MHz, CDCl$_3$) $\delta$ (ppm): 7.88 (1H, s, H$^4$-Ar), 7.31 (1H, d, $J$ = 8.80 Hz, H$^5$-Ar), 6.60 (1H, dd, $J$ = 9.00, 2.60 Hz, H-6), 6.48 (2H, dd, $J$ = 12.0, 5.20 Hz, H$^6$-Ar, H$^8$-Ar), 6.23 (1H, d, $J$ = 8.6 Hz, H-7), 5.19 (2H, *m*, H-22, H-23), 4.98–4.86 (1H, m, -O<u>H</u>), 3.71 (2H, s, -C<u>H</u>$_2$CH$_3$), 3.54 (4H, s, -NC<u>H</u>$_2$CH$_2$N-), 3.45 (4H, q, $J$ = 7.20 Hz, -NCH$_2$C<u>H</u>$_2$N-), 3.37 (2H, s, -C<u>H</u>$_2$CH$_3$), 2.18 (1H, d, $J$ = 4.60 Hz), 2.02 (4H, m), 1.85 (1H, d, $J$ = 7.00 Hz), 1.76-1.69 (1H, m), 1.63 (4H, m), 1.59 (2H, dd, $J$ = 13.0, 5.8 Hz), 1.52 (2H, t, $J$ = 6.2 Hz), 1.39–1.35 (1H, m), 1.25 (4H, d, $J$ = 5.20 Hz), 1.23 (6H, m, 2 × -C<u>H</u>$_3$), 1.01 (3H, m, -C<u>H</u>$_3$), 0.90 (6H, m, 2 × -CH$_2$C<u>H</u>$_3$), 0.81 (9H, m, 3 × -C<u>H</u>$_3$). $^{13}$C-NMR (100 MHz, CDCl$_3$) $\delta$ (ppm): 165.2, 159.2, 157.3, 154.6, 151.8, 135.1, 135.1, 132.4, 130.9, 130.0, 115.7, 109.4, 107.8, 97.0, 81.9, 79.4, 70.9, 56.3, 51.7, 51.1, 50.0, 44.6, 42.8, 39.7, 39.4, 37.0, 34.4, 33.5, 33.1, 28.7, 23.3, 21.0, 19.8, 19.6, 18.0, 17.6, 12.9, 12.4. MS (ESI) *m/z*: 784.5 [M + H]$^+$

### 3.2. Biological Evaluation

#### 3.2.1. Cell Culture

Cancer cell lines (HepG2, SK-Hep1, and MCF-7) were obtained from the College of Pharmacy, Qiqihar Medical University. Cells were cultured in DMEM medium (HepG2 and SK-Hep1) or RPMI 1640 medium (MCF-7) supplemented with 10% FBS and 1% penicillin/streptomycin and maintained in an incubator with a humidified atmosphere of 5% CO$_2$ at 37 °C [23].

#### 3.2.2. MTT Assay

The effects of compounds on cell viabilities of HepG2, SK-Hep1, and MCF-7 cells were evaluated by an MTT assay. Exponentially growing cells were seeded at a density of $2 \times 10^4$ cells/mL into 96-well plates and cultured for 24 h. The tested samples at gradient concentrations (0.5, 1, 10, 20, 50, and 100 μM) were solubilized in DMSO. Then, the cells were treated with samples for 48 h and 10 μL of MTT (KeyGEN Biotech, Nanjing, China) was added for an extra 2 h. Control cells were treated with vehicle alone. The formazan dye product was measured on a Spectra Max 340 microplate reader at 490 nm (Thermo Multiskan MK3, Thermo Electron Corporation, Waltham, MA, USA). The IC$_{50}$ values of all compounds were calculated using SPSS 17.0 software (SPSS, Chicago, IL, USA).

#### 3.2.3. Living Cell Staining for Subcellular Localization

HepG2 cells were incubated on glass cover-slips in 6-well plate ($4 \times 10^5$ cells/2 mL of medium for per well). After removing the medium, the cells were incubated with probe **8d** (5 μM and 10 μM) (in 2 mL of HBSS buffer per well) for 2 h, and then Rh123 (100 nM) was added in the last 30 min. After removing of HBSS buffer and three times of wash with PBS, the cells were fixed with 4% paraformaldehyde for 10 minutes and washed with PBS for three times. At last, the cover-slips were sealed strictly with nail polish for imaging.

#### 3.2.4. Confocal Microscopic Imaging

Confocal images were obtained with confocal microscopy (LSM 510, Carl Zeiss, Oberkochen, Germany), original magnification 100×. The excitation at 579 nm was used for Rh123 dye. For probe **8d**, the excitation laser was 404 nm, and the images were collected at the emission of 470 nm. The colocalization analysis of probe **8d** and Rh123 on images were processed by LSM 510 software (Carl Zeiss, Oberkochen, Germany).

#### 3.2.5. Cell Cycle Analysis

The HepG2 cells were cultivated at a concentration of $5 \times 10^5$ cells/mL into 6-well plates with probe **8d** (3 μM) for 24 h. The cells were washed in PBS and centrifuged for 5 min at 350 g (Eppendorf 5804R, Hamburg, Germany) The collected pellets were incubated at a concentration of $10^6$ cells/mL

with propidium iodide (PI, BD Pharmingen, BD Biosciences, San Jose, CA, USA) staining solution (50 µg/mL in PBS) for 30 min. The cells cycle was analyzed with flow cytometry (BD Biosciences).

### 3.2.6. Colony, Invasion, And Migration Analysis

Colony formation: HepG2 cells (500 cells/well) were mixed with low melting agarose gel (0.25%). Then, probe **8d** (7 µM) was added into 6-well plates and maintained in 5% $CO_2$ incubator for two weeks. The colonies of cells were counted and stained, and then the photograph was analyzed under an optics microscope. Migration: HepG2 cells ($3 \times 10^4$) were mixed in RPMI 1640 media (200 µL) and added to the upper chamber of transwell apparatus (8 µm pore size, COSTAR transwell, Corning, NY, USA). The cells were treated with **8d** (7 µM) for 20 h. Cells that migrated to the lower chamber were stained using crystal violet, and then the number of cells in three different high-power fields (×100) was counted. Invasion: the upper chamber of transwell was coated using a layer of the extracellular matrix. HepG2 cells ($1 \times 10^5$) were added to the upper chamber and treated with **8d** (7 µM) for 24 h. Then, the cells were stained and counted that invaded to the lower chamber in the same way as migration.

### 3.2.7. Measurement of Intracellular ROS in HepG2 Cells

The production of ROS was measured using CM-$H_2$DCFDA (Sigma-Aldrich, Milan, Italy). Briefly, HepG2 cells ($5 \times 10^5$) were seeded in 6 cm dishes and exposed to compound **8d** for 24 h at serial concentrations (0, 5, and 20 µM), after which the medium was removed, and washed with PBS, followed by incubation with 10 µM CM-$H_2$DCFDA for 30 min at 37 °C in serum-free medium. Then, the incubation medium containing CM-$H_2$DCFDA was removed, washed with PBS, and the cells were trypsinized and resuspended in PBS buffer. The quantity of ROS was monitored by flow cytometer (BD Biosciences), with dual channes fluorescence (DCF) luorescence detection channel.

## 4. Conclusions

In summary, we have successfully designed and prepared four mitochondria-targeting theranostic probes **8a–d** by direct conjugation of a coumarin-3-carboxamide fluorophore with ergosterol peroxide **1**. The cytotoxicities of synthesized conjugates against three human tumor cell lines (HepG2, SK-Hep1, and MCF-7) were investigated. The results of fluorescent imaging showed that the synthesized conjugates **8a–d** localized and enriched mainly in mitochondria, leading to significantly enhanced cytotoxicity over ergosterol peroxide. The biological functions of probe **8d** showed that it inhibited cell colony formation, invasion, and migration; induced G2/M phase arrest of HepG2 cells, and increased the intracellular ROS level. The present work provides new information to the potential of ergosterol peroxide as a drug lead compound for the versatile interest of research on steroidal anticancer agents. Besides, the strategy of natural products to mitochondria with enhanced cytotoxicity is in contrast to the well-established methods of using drug-mediated fluorophore delivery and may represent a feasible method for the design of theranostic probes.

## Abbreviations

| | |
|---|---|
| HepG2, SK-Hep1 | Human liver carcinoma cell line |
| MCF-7 | human breast adenocarcinoma cell line |
| DCC | dicyclohexylcarbodi imide |
| HOBT | 1-hydroxylbenzotriazole |
| DMAP | 4-dimethylaminopyridine |
| EDCI | 1-ethyl-3-(3-dimethylaminopropyl)carbodiimide |
| PNPFC | 4-nitrophenyl chloroformate |
| CM-H2DCFDA | 5-(and-6)-chlorometry-2′,7′-dichlorodihydro-fluorescein diacetate acetyl ester |
| TBTU | 2-(1H-Benzotriazole-1- yl)-1,1,3,3-tetramethyluronium tetrafluoroborate |
| DIPEA | N,N-diisopropylethylamine |

## References

1. Bu, M.; Yang, B.B.; Hu, L. Natural Endoperoxides as Drug Lead Compounds. *Curr. Med. Chem* **2016**, *23*, 383–405. [CrossRef] [PubMed]

2. Cui, J.; Liu, L.; Zhao, D.; Gan, C.; Huang, X.; Xiao, Q.; Qi, B.; Yang, L.; Huang, Y. Synthesis, characterization and antitumor activities of some steroidal derivatives with side chain of 17-hydrazone aromatic heterocycle. *Steroids* **2015**, *95*, 32–38. [CrossRef] [PubMed]

3. Plaza-Parrochia, F.; Romero, C.; Valladares, L.; Vega, M. Endometrium and steroids, a pathologic overview. *Steroids* **2017**, *126*, 85–91. [CrossRef] [PubMed]

4. Zaki, A.A.; Ali, Z.; Wang, Y.-H.; El-Amier, Y.A.; Khan, S.I.; Khan, I.A. Cytotoxic steroidal saponins from Panicum turgidum Forssk. *Steroids* **2017**, *125*, 14–19. [CrossRef]

5. Callaway, E.; Cyranoski, D. Anti-parasite drugs sweep Nobel prize in medicine 2015. *Nat. News* **2015**, *526*, 174–175. [CrossRef]

6. Jung, M.; Kim, H.; Lee, K.; Park, M. Naturally Occurring Peroxides with Biological Activities. *Mini-Reviews Med. Chem.* **2003**, *3*, 159–165. [CrossRef]

7. Imamura, Y.; Yukawa, M.; Ueno, M.; Kimura, K.-I.; Tsuchiya, E. 3,6-Epidioxy-1,10-bisaboladiene inhibits G1-specific transcription through Swi4/Swi6 and Mbp1/Swi6 via the Hog1 stress pathway in yeast. *FEBS J.* **2014**, *281*, 4612–4621. [CrossRef]

8. He, F.; Pu, J.X.; Huang, S.X.; Wang, Y.Y.; Xiao, W.L.; Li, L.M.; Liu, J.P.; Zhang, H.B.; Li, Y.; Sun, H.D. Schinalactone A, a new cytotoxic triterpenoid from Schisandrasphenanthera. *Org. Lett.* **2010**, *12*, 1208–1211. [CrossRef]

9. Li, H.; Huang, H.; Shao, C.; Huang, H.; Jiang, J.; Zhu, X.; Liu, Y.; Liu, L.; Lu, Y.; Li, M.; et al. Cytotoxic Norsesquiterpene Peroxides from the Endophytic FungusTalaromyces flavusIsolated from the Mangrove PlantSonneratia apetala. *J. Nat. Prod.* **2011**, *74*, 1230–1235. [CrossRef]

10. Noori, S.; Hassan, Z.M. Tehranolide inhibits cell proliferation via calmodulin inhibition, PDE, and PKA activation. *Tumor Biol.* **2014**, *35*, 257–264. [CrossRef]

11. Kim, D.-H.; Jung, S.J.; Chung, I.-S.; Lee, Y.-H.; Kim, D.-K.; Kim, S.-H.; Kwon, B.-M.; Jeong, T.-S.; Park, M.-H.; Seoung, N.-S.; et al. Ergosterol Peroxide from Flowers of Erigeron annuus L. as an Anti-Atherosclerosis Agent. *Arch. Pharmacal Res.* **2005**, *28*, 541–545. [CrossRef]

12. Nowak, R.; Drozd, M.; Mendyk, E.; Lemieszek, M.; Krakowiak, O.; Kisiel, W.; Rzeski, W.; Szewczyk, K. A new method for the isolation of ergosterol and peroxyergosterol as active compounds of hygrophoropsis aurantiaca and in vitro antiproliferative activity of isolated ergosterol peroxide. *Molecules* **2016**, *21*, 946. [CrossRef] [PubMed]

13. Kobori, M.; Yoshida, M.; Ohnishi-Kameyama, M.; Shinmoto, H. Ergosterol peroxide from an edible mushroom suppresses inflammatory responses in RAW264.7 macrophages and growth of HT29 colon adenocarcinoma cells. *Br. J. Pharmacol.* **2007**, *150*, 209–219. [CrossRef] [PubMed]

14. Wu, Q.-P.; Xie, Y.-Z.; Deng, Z.; Li, X.-M.; Yang, W.; Jiao, C.-W.; Fang, L.; Li, S.-Z.; Pan, H.-H.; Yee, A.J.; et al. Ergosterol Peroxide Isolated from Ganoderma lucidum Abolishes MicroRNA miR-378-Mediated Tumor Cells on Chemoresistance. *PLoS ONE* **2012**, *7*, e44579. [CrossRef] [PubMed]

15. Fang, S.-T.; Liu, X.; Kong, N.-N.; Liu, S.-J.; Xia, C.-H. Two new withanolides from the halophyte Datura stramonium L. *Nat. Prod. Res.* **2013**, *27*, 1965–1970. [CrossRef] [PubMed]

16. Ye, G.; Fu, G.; Yang, B.B.; Zhao, S.; Cheng, J.-X.; Peng, C. Ganoderma lucidum exerts anti-tumor effects on ovarian cancer cells and enhances their sensitivity to cisplatin. *Int. J. Oncol.* **2011**, *38*, 1319–1327.

17. Han, J.; Sohn, E.J.; Kim, B.; Kim, S.; Won, G.; Yoon, S.; Lee, J.; Kim, M.J.; Lee, H.; Chung, K.; et al. Upregulation of death receptor 5 and activation of caspase 8/3 play a critical role in ergosterol peroxide induced apoptosis in DU 145 prostate cancer cells. *Cancer Cell Int.* **2014**, *14*, 117. [CrossRef]

18. Zhu, R.; Zheng, R.; Deng, Y.; Chen, Y.; Zhang, S. Ergosterol peroxide from Cordyceps cicadae ameliorates TGF-β1-induced activation of kidney fibroblasts. *Phytomedicine* **2014**, *21*, 372–378. [CrossRef] [PubMed]

19. Rhee, Y.-H.; Jeong, S.-J.; Lee, H.-J.; Lee, H.-J.; Koh, W.; Jung, J.H.; Kim, S.-H.; Sung-Hoon, K. Inhibition of STAT3 signaling and induction of SHP1 mediate antiangiogenic and antitumor activities of ergosterol peroxide in U266 multiple myeloma cells. *BMC Cancer* **2012**, *12*, 28. [CrossRef]

20. Bu, M.; Cao, T.; Li, H.; Guo, M.; Yang, B.B.; Zeng, C.; Hu, L. Synthesis of 5α,8α-Ergosterol Peroxide 3-Carbamate Derivatives and a Fluorescent Mitochondria-Targeting Conjugate for Enhanced Anticancer Activities. *ChemMedChem* **2017**, *12*, 466–474. [CrossRef]

21. Bu, M.; Cao, T.; Li, H.; Guo, M.; Yang, B.B.; Zeng, C.; Zhou, Y.; Zhang, N.; Hu, L. Synthesis and biological evaluation of novel steroidal 5α,8α-epidioxyandrost-6-ene-3β-ol-17-(O-phenylacetamide)oxime derivatives as potential anticancer agents. *Bioorganic Med. Chem. Lett.* **2017**, *27*, 3856–3861. [CrossRef] [PubMed]

22. Bu, M.; Cao, T.; Li, H.; Guo, M.; Yang, B.B.; Zhou, Y.; Zhang, N.; Zeng, C.; Hu, L. Synthesis and biological evaluation of novel steroidal 5α,8α-endoperoxide derivatives with aliphatic side-chain as potential anticancer agents. *Steroids* **2017**, *124*, 46–53. [CrossRef] [PubMed]

23. Li, X.; Wu, Q.; Bu, M.; Hu, L.; Du, W.W.; Jiao, C.; Pan, H.; Sdiri, M.; Wu, N.; Xie, Y.; et al. Ergosterol peroxide activates Foxo3-mediated cell death signaling by inhibiting AKT and c-Myc in human hepatocellular carcinoma cells. *Oncotarget* **2016**, *7*, 33948–33959. [CrossRef] [PubMed]

24. Jia, M.; Zhao, R.; Xu, B.; Yan, W.; Chu, F.; Gu, H.; Xie, T.; Xiang, H.; Ren, J.; Chen, D.; et al. Synthesis and biological activity evaluation of novel peroxo-bridged derivatives as potential anti-hepatitis B virus agents. *MedChemComm* **2016**, *8*, 148–151. [CrossRef] [PubMed]

25. Kovacic, P.; Somanathan, R. Recent developments in the mechanism of anticancer agents based on electron transfer, reactive oxygen species and oxidative stress. *Anti-Cancer Agents Med. Chem.* **2011**, *11*, 658–668. [CrossRef]

26. Li-Weber, M. Targeting apoptosis pathways in cancer by Chinese medicine. *Cancer Lett.* **2013**, *332*, 304–312. [CrossRef] [PubMed]

27. Bauch, M.; Klaper, M.; Linker, T. Intermediates in the cleavage of endoperoxides. *J. Phys. Org. Chem.* **2016**, *30*, e3607. [CrossRef]

28. Florean, C.; Song, S.; Dicato, M.; Diederich, M. Redox biology of regulated cell death in cancer: A focus on necroptosis and ferroptosis. *Free. Radic. Boil. Med.* **2019**, *134*, 177–189. [CrossRef] [PubMed]

29. Ling, T.; Lang, W.H.; Martinez-Montemayor, M.M.; Rivas, F. Development of ergosterol peroxide probes for cellular localisation studies. *Org. Biomol. Chem.* **2019**, *17*, 5223–5229. [CrossRef] [PubMed]

30. Jin, H.; Ko, Y.S.; Park, S.W.; Chang, K.C.; Kim, H.J. 13-Ethylberberine Induces Apoptosis through the Mitochondria-Related Apoptotic Pathway in Radiotherapy-Resistant Breast Cancer Cells. *Molecules* **2019**, *24*, 2448. [CrossRef] [PubMed]

31. Zhang, X.; Ba, Q.; Gu, Z.; Guo, D.; Zhou, Y.; Xu, Y.; Wang, H.; Ye, D.; Liu, H. Fluorescent Coumarin-Artemisinin Conjugates as Mitochondria-Targeting Theranostic Probes for Enhanced Anticancer Activities. *Chem. - A Eur. J.* **2015**, *21*, 17415–17421. [CrossRef] [PubMed]

32. Caputo, C.A.; Gross, M.A.; Lau, V.W.-H.; Cavazza, C.; Lotsch, B.V.; Reisner, E. Photocatalytic Hydrogen Production using Polymeric Carbon Nitride with a Hydrogenase and a Bioinspired Synthetic Ni Catalyst**. *Angew. Chem.* **2014**, *126*, 11722–11726. [CrossRef] [PubMed]

33. Liu, Y.; Lok, C.-N.; Ko, B.C.-B.; Shum, T.Y.-T.; Wong, M.K.; Che, C.-M. Subcellular Localization of a Fluorescent Artemisinin Derivative to Endoplasmic Reticulum. *Org. Lett.* **2010**, *12*, 1420–1423. [CrossRef] [PubMed]

34. Sun, T.; Guan, X.; Zheng, M.; Jing, X.; Xie, Z. Mitochondria-Localized Fluorescent BODIPY-Platinum Conjugate. *ACS Med. Chem. Lett.* **2015**, *6*, 430–433. [CrossRef] [PubMed]

35. Wu, S.; Cao, Q.; Wang, X.; Cheng, K.; Cheng, Z. Design, synthesis and biological evaluation of mitochondria targeting theranostic agents. *Chem. Commun.* **2014**, *50*, 8919–8922. [CrossRef] [PubMed]

36. Kumar, R.; Han, J.; Lim, H.-J.; Ren, W.X.; Lim, J.-Y.; Kim, J.-H.; Kim, J.S. Mitochondrial Induced and Self-Monitored Intrinsic Apoptosis by Antitumor Theranostic Prodrug: In Vivo Imaging and Precise Cancer Treatment. *J. Am. Chem. Soc.* **2014**, *136*, 17836–17843. [CrossRef] [PubMed]
37. Hu, Q.; Gao, M.; Feng, G.; Liu, B. Mitochondria-Targeted Cancer Therapy Using a Light-Up Probe with Aggregation-Induced-Emission Characteristics. *Angew. Chem.* **2014**, *126*, 14449–14453. [CrossRef]
38. Chao, W.; Lv, W.; Zhen, X.; Long, Y. A fret-based fluorescent probe for imaging H2S in living cells. *Tetrahedron Lett.* **2013**, *54*, 6937–6939.
39. Xie, H.; Mire, J.; Kong, Y.; Chang, M.; Hassounah, H.A.; Thornton, C.N.; Sacchettini, J.C.; Cirillo, J.D.; Rao, J. Rapid point-of-care detection of the tuberculosis pathogen using a BlaC-specific fluorogenic probe. *Nat. Chem.* **2012**, *4*, 802–809. [CrossRef] [PubMed]
40. Wang, L.-H.; Chang, G.-Q.; Zhang, H.-J.; Wang, J.; Lin, Y.-N.; Jin, W.-N.; Li, H.-W.; Gao, W.; Wang, R.-J.; Li, Q.-H.; et al. Neutrophil gelatinase-associated lipocalin regulates intracellular accumulation of Rh123 in cancer cells. *Genes Cells* **2012**, *17*, 205–217. [CrossRef]
41. Wang, H.; Joseph, J.A. Quantifying cellular oxidative stress by dichlorofluorescein assay using microplate reader. *Free Radic. Biol. Med.* **1999**, *27*, 612–616. [CrossRef]

**Sample Availability:** Samples of the compounds **8a–d** are available from the authors.